ACS APPLIED MATERIALS & INTERFACES

Research Article

www.acsami.org

Preparation, Characterization, and Antibacterial Activity of Silver Nanoparticle-Decorated Graphene Oxide Nanocomposite

Wei Shao,*[,†] Xiufeng Liu,[‡] Huihua Min,[§] Guanghui Dong,[†] Qingyuan Feng,[†] and Songlin Zuo*[,†]

[†]College of Chemical Engineering, Nanjing Forestry University, Nanjing 210037, P. R. China

[‡]College of Life Science, Nanjing University, Nanjing 210093, P. R. China

[§]Advanced Analysis and Testing Center, Nanjing Forestry University, Nanjing 210037, P. R. China

ABSTRACT: In this work, we report a facile and green approach to prepare a uniform silver nanoparticles (AgNPs) decorated graphene oxide (GO) nanocomposite (GO-Ag). The nanocomposite was fully characterized by transmission electron microscopy (TEM), Fourier transform infrared (FTIR) spectra, ultraviolet−visible (UV−vis) absorption spectra, and X-ray photoelectron spectroscopy (XPS), which demonstrated that AgNPs with a diameter of approximately 22 nm were uniformly and compactly deposited on GO. To investigate the silver ion release behaviors, HEPES buffers with different pH (5.5, 7, and 8.5) were selected and the mechanism of release actions was discussed in detail. The cytotoxicity of GO-Ag nanocomposite was also studied using HEK 293 cells. GO-Ag nanocomposite displayed good cytocompatibility. Furthermore, the antibacterial properties of GO-Ag nanocomposite were studied using Gram-negative *E. coli* ATCC 25922 and Gram-positive *S. aureus* ATCC 6538 by both the plate count method and disk diffusion method. The nanocomposite showed excellent antibacterial activity. These results demonstrated that GO-Ag nanocomposite, as a kind of antibacterial material, had a great promise for application in a wide range of biomedical applications.

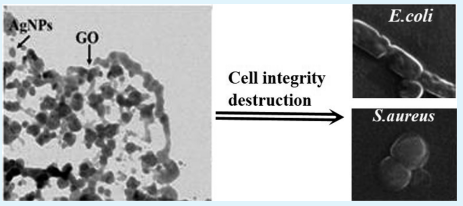

KEYWORDS: *graphene oxide, silver, silver release behavior, cytotoxicity, antibacterial*

INTRODUCTION

Microorganisms can be easily found in environments, such as air, ocean, or soil. Once bacteria attach to a surface, a multistep process starts leading to the formation of a complex, adhering microbial community that is termed a biofilm. Once a biofilm has formed, it is very difficult to treat clinically because the bacteria on the interior of the biofilm are protected from phagocytosis and antibiotics.[1] The presence of biofilms can cause mechanical blockage in fluid systems, disturbances of heat transfer processes and corrosion in metallic surfaces in industrial process. Moreover, it can lead to severe hygienic problems and even serious diseases when pathogens are involved in the food industry. In particular, it can also cause medical device-associated infections.[2−4] Therefore, antibacterial materials and agents play an increasingly important role in combating microorganisms. However, conventional antibiotic therapies were becoming less efficient owing to the wide use of antibiotics and the emergence of antibiotic-resistant bacterial strains, resulting in poor treatment efficacy and the significantly increasing cost of healthcare.[5,6] Thereby, the demand of developing new generations of antimicrobial agents for effectively killing pathogenic bacteria is becoming crucial.

Silver and silver-based compounds exhibit a strong antibacterial activity to a wide range of microorganisms which have been used extensively in many bactericidal applications.[7] Silver nanoparticles (AgNPs) are nontolerant disinfectants that can significantly reduce many bacterial infections with long duration compared with the widespread usage of biocides, such as benzyl penicillin, tetracycline, etc. Some bacteria are naturally resistant to some antibiotics, and some have developed resistance to antibiotics. For examples, *Neisseris gonorrhoeae* (*N. gonorrhoeae*) and *Staphylococcus aureus* (*S. aureus*) are resistant to benzyl penicillin. Thereby, AgNPs are attracted great attention since they are effective biocides against numerous kinds of bacteria, fungi, and viruses. The mechanism of bactericidal effect of AgNPs against bacteria is not very clear. It has been proposed that the antibacterial activity is based on the electrostatic attraction between negative charged cell membrane of microorganism and positive charged Ag ion. Therefore, Ag^+ can cause bacterial cell death by damaging the cell membrane, strongly interacts with thiol groups of vital enzymes and destroying DNA replication ability.[3,8] It is well-known that the antibacterial activity of AgNPs is strongly related to their size and distribution.[9] However, AgNPs with small size tend to aggregate to minimize their surface energy in the process of preparation, which led to a remarkable deterioration of their antibacterial properties. To overcome this shortcoming, it is crucial to find a proper support material to load AgNPs efficiently.[10]

Graphene oxide (GO), a well-known monolayers of carbon atoms that form dense honeycomb structures containing hydroxyl and epoxide functional groups on the two accessible sides and carboxylic groups at the edges.[11] Moreover, it has unique properties including large surface area, low cytotoxicity,

Received: January 31, 2015
Accepted: March 11, 2015
Published: March 11, 2015

DOI: 10.1021/acsami.5b00937
ACS Appl. Mater. Interfaces 2015, 7, 6966−6973

and good water stability. Hence, it can act as the platform for growing metal nanoparticles and stabilizing them.[12] On the basis of these, GO and its composites have a wide range of potential applications on transistors, transparent conductors, polymer reinforcement, bioengineering, and biomaterials areas.[13−15] Recently, many researches have focus on the antibacterial activity of GO-Ag nanocomposites.[16−18] Accordingly, hydroxyl, epoxide, carbonyl, and carboxyl groups on the basal planes of GO allow AgNPs to interact with GO nanosheets through physisorption, electrostatic binding or charge-transfer interactions.[19] In particular, silver cations can directly attach to the carboxyl groups on the GO surface by electrostatic interactions. Thus, the reduction takes place on the surface of GO nanosheets, forming a stable GO-Ag nanocomposite. By incorporation of GO as the supporter, the aggregation problem of AgNPs can be minimized and even prevented.

Herein, we report a facile, cost-effective, one-pot solution-phase green synthetic method to fabricate AgNPs decorated GO nanocomposite (GO-Ag) with glucose as reducing agent and starch as stabilizer. In addition, antibacterial properties and cytotoxocity tests of as-synthesized materials were also investigated. The resultant GO-Ag nanocomposite shows low cell cytotoxicity and excellent antibacterial activity.

EXPERIMENTAL SECTION

Materials. A common Hummers method was used to synthesize a GO dispersion with a 2 mg/mL concentration using graphite powder provided by XFNANO Materials Tech Co., Ltd. (Nanjing, China). HEPES (Vetec reagent grade) was obtained from Sigma. The other chemicals used in the tests were purchased from Sinopharm Chemical Reagent Co., Ltd. All reagents were of analytical grade and used as received without further purifying.

Preparation of AgNPs Decorated GO Nanocomposite. AgNPs decorated GO (GO-Ag) nanocomposite was prepared by using slight modifications of the procedures developed by Cheviron et al. and Tang et al.[20,21] In this study, 0.2 mL of homogeneous suspension of GO (2 mg/mL) was added into 19.8 mL of deionized water and treated by ultrasonication at a supersonic power of 500 W (YQ-1003A, Ningbo Power Ultrasonic Equipment Co., Ltd., China) for 5 min under ice−water bath. The desired amount of $AgNO_3$ were added into 10 mL of diluted GO suspensions and heated to 80 °C (A) to achieve a concentration of 2 mM. Then 1 mM glucose and 4% starch in another 10 mL of diluted GO suspensions were heated to 80 °C (B). Then B was slowly added into A under vigorous stirring and kept 80 °C for 4 h for the complete reduction. The color of the reaction mixture turns from dark brown to gray and finally dark green. The synthesized GO-Ag nanocomposite was centrifugated at 10 000 rpm for 10 min and repeated washing for three times using deionized water and dried at 70 °C for 12 h to obtain GO-Ag nanocomposite. Then, it was redispersed in deionized water to achieve a concentration of 20 μg/mL for further analysis.

Preparation of AgNPs Colloid. The procedure of preparing AgNPs colloid was similar to that of GO-Ag nanocomposite, except that GO suspension was replaced by deionized water. The finial color of the reaction mixture turns to light yellow. The synthesized AgNPs was centrifugated at 10 000 rpm for 10 min and repeated washing for three times using water and dried at 70 °C for 12 h.

Characterization. The high-resolution transmission electron microscopy (HRTEM) images were taken by a JEM-2100 model instrument operated at an accelerating voltage of 300 kV. Samples for HRTEM imaging were prepared by placing a drop of sample solution in ethanol onto a carbon-coated copper grid and dried in air. The UV−visible absorption spectra were recorded Shimadzu UV-2450 spectrophotometer in the range of 200−600 nm. Fourier-transform infrared (FTIR) spectra were recorded on a Spectrum Two Spectrometer (PerkinElmer) with the wavenumber range of 4000−400 cm^{-1} at a resolution of 4 cm^{-1}. Raman spectra were recorded on a DXR Smart Raman spectrometer (Thermo Fisher) with 532 nm laser excitation. X-ray photoelectron spectroscopy (XPS) measurements were carried out with Thermo Escalab 250Xi instrument (Thermo Fisher) using Al Kα radiation (1486.6 eV, 150 W). The base pressure was less than 10^{-8} Torr. The background in XPS data was subtracted using the Shirley method,[20] and the XPS curve-fitting was performed using a Gaussian function at high resolution. The spectra in the C 1s and N 1s regions were deconvoluted by OriginPro 8 software.

Silver Release Behaviors. The kinetics of silver ion release was studied from the prepared GO-Ag nanocomposite. In order to determine the effect of pH on the silver ion release profiles of the nanocomposite, HEPES (Sigma) buffers with different pH values at 5.5, 7, and 8.5 were used, respectively. The 5 mL tested samples were immersed in a beaker containing 95 mL of 10 mM HEPES at 37 °C and sealed using PARAFILM M. The 1.5 mL solution was taken at regular time intervals (1, 2, 3, 4, 5, 6, 7, 8, 9, and 10 days) and analyzed for the amount of Ag ion released using inductively coupled plasma mass spectrometry NexION 300X (PerkinElmer).

Cytotoxicity Tests. The HEK 293 cell line was cultured in RPMI medium supplemented with 10% FBS, 100 μg/mL penicillin, and 100 μg/mL streptomycin. The cells were then incubated for 3 days in a humidified 5% CO_2-containing balanced-air incubator at 37 °C.

The cytotoxicity was measured using the MTT assay method. A volume of 200 μL of HEK 293 cells, at a density of 1×10^5, were placed in each well of a 48-well plate. Then the cells were incubated overnight at 37 °C in a humidified 5% CO_2-containing atmosphere. After that, the media was discarded. The monolayer of cells in the plate was exposed to various volumes of specimen and then fresh media was added. Wells containing only the cells were used as a control. The cells were treated for another 24 h. Then the media containing sample was changed with fresh media and 20 μL of dimethyl thiazolyl diphenyl (MTT) was added and the incubation continued for 6 h. Medium was removed, and 200 μL of DMSO was added to each well to dissolve the formazan. The absorbance was measured with a test wavelength of 570 nm and a reference wavelength of 630 nm. Empty wells (DMSO alone) were used as blanks. The relative cell viability was measured by comparison with the control well containing only the cells. On the other hand, one part of cells were fixed with 4% paraformaldehyde in PBS for 10 min and then incubated with 2% methanol for 10 min after treated by composites for 24 h. Images were obtained using a microscope (Carl Zeiss, Oberkochen, Germany).

Antibacterial Activity. The antibacterial activity of GO-Ag nanocomposite was investigated against Gram-negative bacteria *Escherichia coli* (*E. coli*) ATCC 25922 and Gram-positive bacteria *S. aureus* ATCC 6538 by two methods: plate count method and disk diffusion method. The strains were cultured in Tryptone Soya Agar (TSA, Oxoid, U.K.) plates in an incubator overnight at 37 °C. A single colony was inoculated in 20 mL of Tryptone Soya Broth (TSB, Oxoid, U.K.) and grown statically overnight at 37 °C. Then, 100 μL of this bacterial suspension was transferred into 100 mL of TSB in a conical flask and grown in a shaker incubator at 150 rpm at 37 °C until the bacteria concentration reached 4×10^6 CFU/mL.

Plate count method. The 100 μL bacterial suspensions were inoculated in conical flasks containing different dosages of GO-Ag dispersions (20, 40, 60, 80, and 100 μL). The final volume in the flasks was 10 mL. The flasks were incubated in a shaker incubator at 100 rpm at 37 °C for 4 h. A control sample was prepared by a similar method without GO-Ag for standard comparison. The 100 μL aliquots of the bacteria suspensions were withdrawn and 10^{-1}, 10^{-2}, and 10^{-3} dilutions were plated out on TSA plates and incubated overnight at 37 °C. The colonies were counted on the following day. The total number of bacteria in 100 μL of bacterial suspension was obtained for each concentration and hence the total number of bacteria after 4 h incubation in the flasks was obtained. The experiments were carried out in triplicate to confirm reproducibility. The antibacterial ratio (R) was calculated using the following equation:

$$R = (N_0 - N_1)/N_0 \times 100\%$$

DOI: 10.1021/acsami.5b00937
ACS Appl. Mater. Interfaces 2015, 7, 6966−6973

where N_0 and N_1 correspond to the number of colonies incubated with the control and GO-Ag nanocomposite, respectively.

Disk diffusion method: different dosages (20, 40, 60, 80, and 100 μL) of GO-Ag nanocomposite aqueous dispersions were added onto a 10 mm filter paper, dried and sterilized by ultraviolet lamp for 60 min. Lawns of test bacteria (1×10^6 CFU/plate) were prepared on TSA. The sterilized samples were then carefully placed upon the lawns and empty filter paper was used as control. The plates were placed in a 37 °C incubator for 24 h. Then inhibitory action of tested samples on the growth of the bacteria was determined by measuring diameter of inhibition zone.

The morphologies characterizations of bacteria were observed with a Quanta 200 SEM (FEI, U.K.). The 1 mL of bacterial suspension was centrifuged at 5000 rpm for 5 min at −4 °C, washed twice with sterile deionized water, followed by fixing with 4% glutaraldehyde solution for 24 h. The samples were dehydrated with sequential treatment of 30, 50, 70, 90, and 100% ethanol for 10 min, then dried by critical point drying, gold sputter-coated, and imaged using SEM.

RESULTS AND DISCUSSION

Characterization of GO-Ag Nanocomposite. In this synthesis procedure of GO-Ag nanocomposites, Ag ions were first loaded onto the surfaces of GO nanosheets. Then, Ag ions were reduced and stabilized by glucose and starch, resulting in the formation of AgNPs on the surfaces of GO nanosheets to form the GO based nanocomposites. Figure 1 presents a schematic diagram to illustrate the one pot preparation of GO-Ag nanocomposite via chemical reduction method.

Transmission electron microscopy (TEM) was used to analyze the morphological aspects of GO and GO-Ag nanocomposite. Figure 2a reveals an almost-transparent single layer GO nanosheet. The AgNPs, represented by dark spots, are shown in Figure 2b. Figure 2c displays a monodisperse layer of spherical-like AgNPs decorating GO nanosheets. TEM

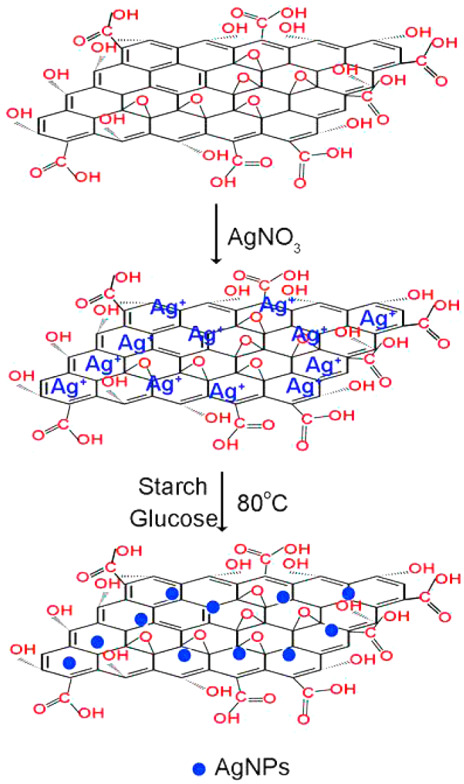

Figure 1. Schematic of the procedure for preparing GO-Ag nanocomposite.

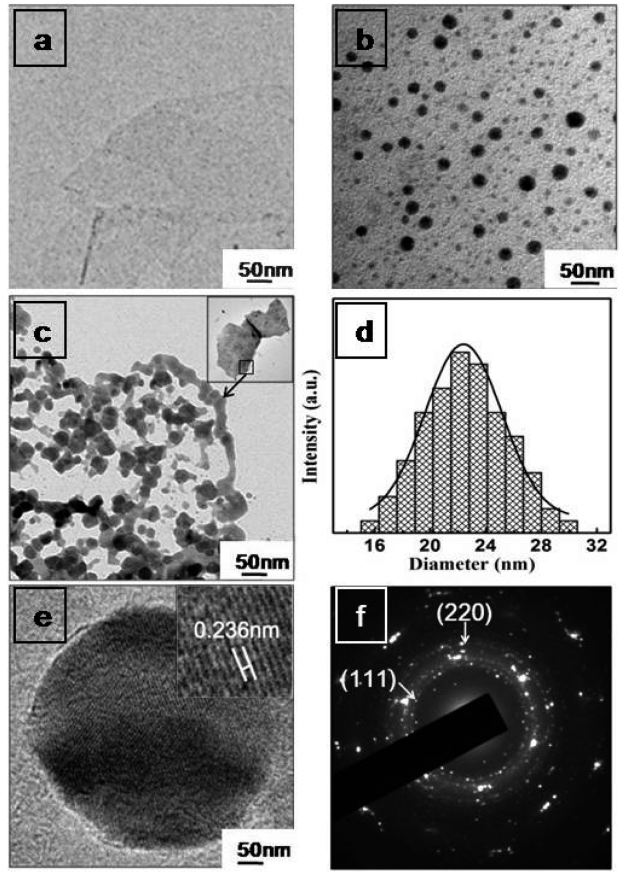

Figure 2. TEM image of GO nanosheets (a), AgNPs (b), GO-Ag nanocomposite (c), size distribution of AgNPs on GO (d), HRTEM of quasi-spherical AgNPs on GO (e), and SED pattern of GO-Ag nanocomposite (f).

image showed that AgNPs (black dots) are spherical and uniformly dispersed on the surface of GO nanosheets. The inset image in Figure 2c is the GO-Ag nanocomposites with lower magnification. The size distribution of deposited AgNPs is relatively narrow and with a mean diameter of about 22 nm (Figure 2d). These results suggest that GO nanosheets play an important role in the process of nucleation and stabilization, allowing the formation of AgNPs. Furthermore, the addition of starch as a stabilizing agent thus helped efficiently in preventing the agglomeration of AgNPs. Meanwhile, GO nanosheets appeared to act as a morphological driver for AgNPs, dictating the formation of spherical-like particles in the GO-Ag nanocomposite.[2]

The crystallinity of AgNPs was further investigated by high-resolution TEM (HRTEM) and selected-area electron diffraction (SAED). HRTEM image (Figure 2e) shows AgNPs were embedded on the surface of GO nanosheets and displayed multitwinned structures. In addition, the measured fringe lattice of AgNPs is 0.236 nm which attributes to the (111) plane. Figure 2f shows a typical SAED pattern of synthesized AgNPs on GO nanosheets, which exhibits multiple-crystal diffraction features. Two visible diffraction rings can be clearly observed and indexed as face centered cubic (FCC) metallic silver. The strongest pattern (inner ring) shows the characteristic diffraction rings corresponding to the (111) plane. The outermost ring is likely attributed to the (220) reflection.[5]

DOI: 10.1021/acsami.5b00937
ACS Appl. Mater. Interfaces 2015, 7, 6966−6973

UV−Visible Spectroscopy. UV−vis spectroscopy was used to monitor the formation of AgNPs on GO-Ag nanocomposite. Two characteristic peaks were observed in the UV−vis spectrum of GO (Figure 3a), including a signal at 232 nm,

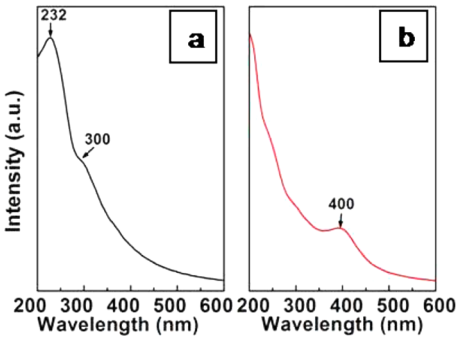

Figure 3. UV−vis absorption spectra of GO (a) and GO-Ag nanocomposite (b).

which ascribes the $\pi-\pi^*$ transitions of the aromatic C−C bonds and a shoulder at 300 nm, which is derived from the $n-\pi^*$ transitions of the C═O bonds.[17,22] As shown in the UV−vis spectra of GO-Ag nanocomposite (Figure 3b), the formation of AgNPs was indicated by the surface plasmon resonance peak of AgNPs at around 400 nm in the GO-Ag nanocomposite, which is similar to previous studies.[18,19] Moreover, it is reported that AgNPs appears spherical shape when its sharp peak is in the range of 400−500 nm,[23] which is consistent with the TEM result.

FTIR Spectroscopy. FTIR measurements were carried out to investigate the interactions between GO and AgNPs. Figure 4 shows the FTIR spectra of GO and GO-Ag nanocomposite.

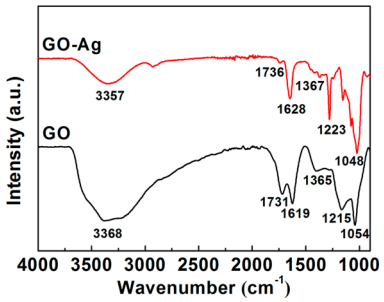

Figure 4. FTIR spectra of GO and GO-Ag nanocomposite.

In the case of GO, the broad and intense peak centered at 3416 cm^{-1}, which is related to the OH groups, and the strong peak at 1728 cm^{-1} corresponds to the stretching vibrations of C═O carboxylic moieties.[24] The peak at 1621 cm^{-1} is associated with the skeletal vibrations of aromatic C═C bond or intramolecular hydrogen bonds.[25] Other bands at 1365, 1215, and 1054 cm^{-1} correspond to C−O−H deformation, C−H stretching (epoxy groups), and C−O stretching vibrations (alkoxy groups), respectively.[26] Therefore, it confirms the existences of the abundance of hydroxyl groups and oxygenous groups on the surface of GO, which makes GO to be convenient for further modification with plasmonic NPs, such as AgNPs.[27]

For GO-Ag nanocomposite, the peak positions of the functional groups on GO still remained, and their shapes were similar. In particular, the intensity of C═O carbonyl stretching (1736 cm^{-1}) decreased, whereas the aromatic C═C vibrations (1628 cm^{-1}) of GO nanosheets increased. This change can prove that there is an interaction between AgNPs and the oxygen-containing functional groups (i.e., −COOH) of GO nanosheets by forming a chemical bond or electrostatic attraction, which was consistent with a similar previous report.[19,28]

XPS Spectroscopy. XPS analysis was performed to investigate the chemical state of GO and GO-Ag nanocomposite. In Figure 5a, the survey spectra clearly indicates the existence of C, O in GO and C, O, Ag in GO-Ag nanocomposite. The C 1s XPS core level spectrum of GO nanosheets is displayed in Figure 5b. It can be deconvoluted into four components with binding energy at 284.8 eV (C═C/C−C in aromatic ring), 286.90 eV (C−O−C), 288.4 eV (C═O), and 289.3 eV (HO−C═O).[21,29] These results indicated that there are a large number of functional groups on the surface of GO nanosheets.

The C 1s and Ag 3d XPS core level spectra of GO-Ag nanocomposite are shown in Figure 5c,d. The C 1s core level XPS spectrum can be deconvoluted into four components with binding energies at 285.0, 287.1, 288.5, and 289.3 eV assigned to C═C, C−O, C═O, and HO−C═O, respectively (Figure 5c). The intensity of the band at 287.1 eV (C−O) decreased which indicates the partial reduction of GO nanosheets to graphene nanosheets. As shown in Figure 5d, XPS spectra clearly show the concision of elemental Ag and the elemental status of Ag (3d). The Ag (3d) peaks are a doublet which arises from spin−orbit coupling ($3d_{5/2}$ and $3d_{3/2}$).[23] The binding energies of Ag $3d_{5/2}$ and Ag $3d_{3/2}$ peaks are 368.76 and 374.79 eV, respectively, which prove clearly that silver is present only in metallic form, indicating the formation of AgNPs on the surface of GO nanosheets.[30]

Raman Spectroscopy. Raman spectroscopy is one of the most powerful and informative techniques to investigate disorder sp^2 carbon material. Raman spectrum of GO (Figure 6a) is characterized by the presence of D band at 1320 cm^{-1} assigning to the breathing mode of κ-point phonons with A_{1g} symmetry, and the G band 1570 cm^{-1} attributed to the tangential stretching mode of the E_{2g} phonon of the carbon sp^2 atoms.[27] The prominent D peak was from the structural imperfections created by the attachment of hydroxyl and epoxide groups on the carbon basal plane.[16] For the spectra of the GO-Ag nanocomposite (Figure 6b), the intensity of both the D and G bands increased after the formation of AgNPs on the surface of the GO nanosheets. This increase can be attributed to the surface-enhanced Raman scattering (SERS) effect.[19] Furthermore, the ratio of the intensities of the D band and G bands were calculated. After the formation of AgNPs on GO, the I_D/I_G ratio increased from 0.86 to 0.97. The increase may be related to an increase in the degree of disorder of the GO matrix, in part due to chemical bonds between the GO matrix and AgNPs.[2]

Silver Ion Release in Vitro. The assessment of silver specific migration is fundamental when evaluating the possible application of the GO-Ag antimicrobial system. The release of antibacterial silver ions can highly depend on the moisture content or the pH of the surrounding environment.[31,32]

In order to evaluate the silver ion release of GO-Ag nanocomposite, the release behaviors were monitored on a daily basis in 10 mM HEPES buffer at different pH values. Acidic (pH = 5.5), neutral (pH = 7), and alkaline (pH = 8.5) conditions were chosen to further assess the effect of pH on

DOI: 10.1021/acsami.5b00937
ACS Appl. Mater. Interfaces 2015, 7, 6966−6973

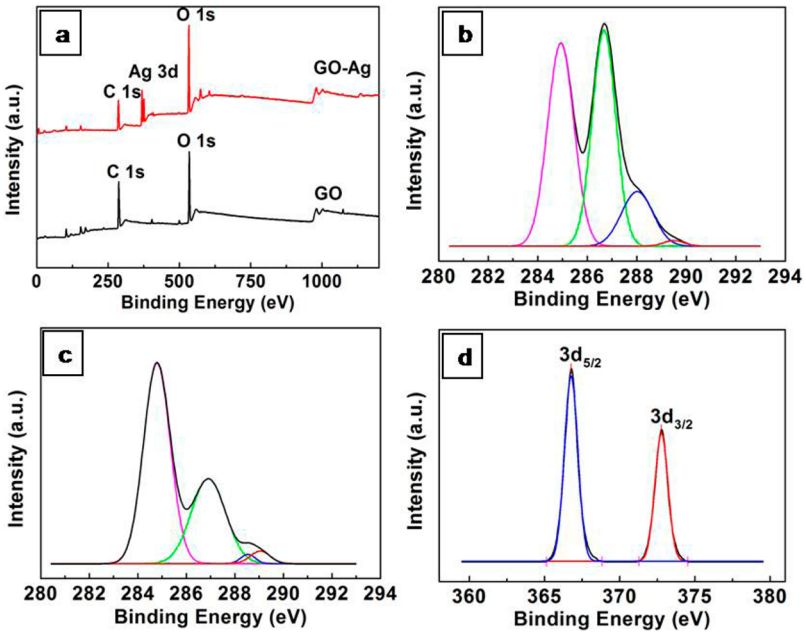

Figure 5. XPS survey scans of GO and GO-Ag (a), C 1s XPS spectra of GO nanosheets (b) and GO-Ag (c), and Ag 3d core level spectrum of GO-Ag (d).

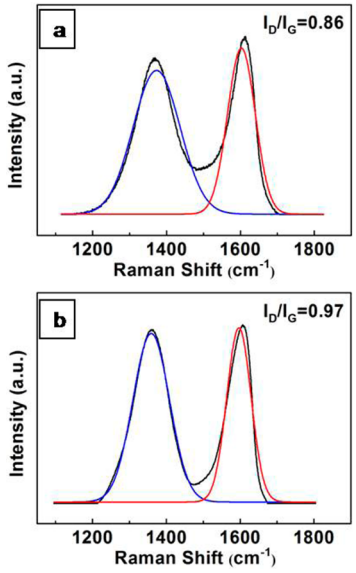

Figure 6. Raman spectra of GO (a) and GO-Ag nanocomposite (b).

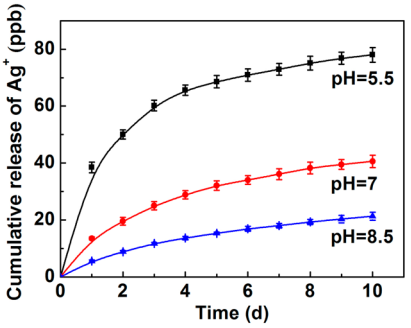

Figure 7. Cumulative release profiles of Ag^+ from GO-Ag nanocomposite in 10 mM HEPES at different pH values: pH = 5.5, pH = 7, and pH = 8.5.

release behavior. As can be observed in Figure 7, the release is in many cases more rapid in the first stage and then a lower release capacity is noted. Meanwhile, higher silver ion concentrations were observed under lower pH value in HEPES buffer systems. This suggested that the silver ion release was strongly pH dependent, and ion release rates decreased with increasing pH, which was in accordance with the previous study.[33,34] In aqueous solutions, there is a possibility of the release of Ag^+ due to the oxidation by dissolved oxygen. The dissolution of AgNPs due to oxygen may be expressed by the following formula:[35]

$$4Ag(s) + O_2(aq) + 4H^+ = 4Ag^+(aq) + 2H_2O(l)$$

On the basis of the above equation, the release of Ag^+ is directly proportional to the extent of Ag oxidation. Lower pH values lead to higher H^+ concentration formed in the medium, which could explain our results that more Ag^+ released from GO-Ag nanocomposite and is consistent with other researchers' works.[33,36] These results demonstrate that GO-Ag nanocomposite has different silver ion release behaviors in an acidic or an alkaline aqueous environment, which can meet the requirement for different applications.

Cytotoxicity. Cytotoxicity studies were performed to investigate the effect of GO-Ag dosage on proliferation of HEK 293 cell line. It is important to determine the effective nanocomposite dosage *in vitro*, since cytocompatibility for materials can be used to assess the potential of materials for application in tissue engineering.[37] The cell viability of HEK 293 cells was evaluated by MTT assay. Different dosages of GO-Ag nanocomposite were added in the well of a 48-well plate containing the same amount of HEK 293 cells. After 24 h incubation, cells were fixed and the cell morphologies were observed by a microscope. Figure 8a–f shows the morphologies of the HEK 293 cells after 24 h culture with different GO-Ag dosages. There are no obvious differences in cell morphologies between the control and tested nanocomposites with different dosages. Cells of the control are very similar to that of the

DOI: 10.1021/acsami.5b00937
ACS Appl. Mater. Interfaces 2015, 7, 6966–6973

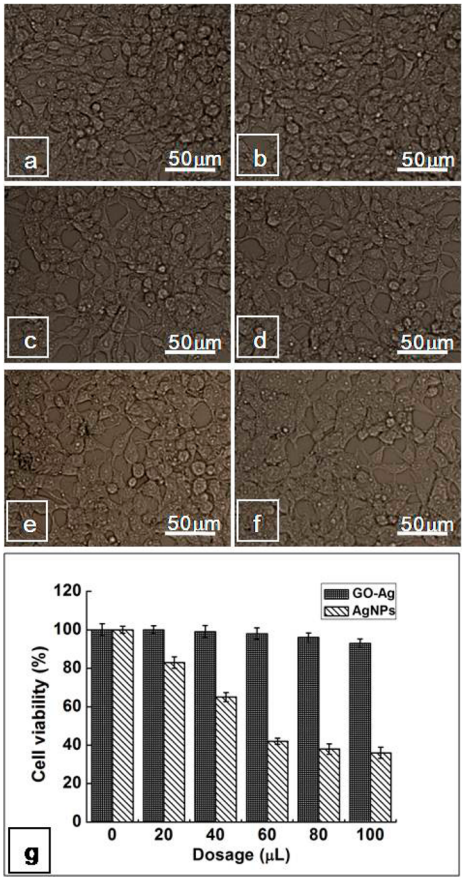

Figure 8. Cell morphologies after 24 h culture with different dosages of GO-Ag nanocomposite: 0 μL (a), 20 μL (b), 40 μL (c), 60 μL (d), 80 μL (e), 100 μL (f), cell viability percentage treated with different dosages of AgNPs and GO-Ag nanocomposite (g).

nanocomposite which display typical fibroblast-like morphology. The MTT result was illustrated in Figure 8g as relative viability of the cells by comparison with the control well containing only the cells. AgNPs significantly inhibited cell proliferation of HEK 293 cells from 20 to 100 μL after 24 h incubation. However, 20−60 μL dosages of GO-Ag nanocomposite showed negligible toxicity on HEK 293 cells. No reduced cell viability following their incubation was shown. The results showed that less than 60 μL dosages of GO-Ag nanocomposite do not inhibit the proliferation of HEK 293 cells. HEK 293 cells viabilities were slightly affected after their incubation with GO-Ag nanocomposites at a higher dosage because the cell viability decreased to 96% and 93% for 80 and 100 μL dosages of GO-Ag nanocomposite, respectively.

Antibacterial Activity. Two strains including Gram-negative *E. coli* ATCC 25922 and Gram-positive *S. aureus* ATCC 6538 were selected for antibacterial tests because they are usually associated with the medical-associated infections.[2] Antibacterial property of GO-Ag nanocomposite was investigated by calculating antibacterial ratios based on the numbers of bacteria colonies incubated with different dosages of GO-Ag nanocomposite at 37 °C after a contact time of 1 h, as shown in Figure 9a,b. It was found that the antibacterial ratio increased with increasing GO-Ag nanocomposite dosages. Anti-*E. coli* ratio of 60 μL dosage of GO-Ag nanocomposite reached 98.36%, and the anti-*S. aureus* ratio was 96.18%, respectively. Antibacterial ratios were 100% with more than 60 μL dosage.

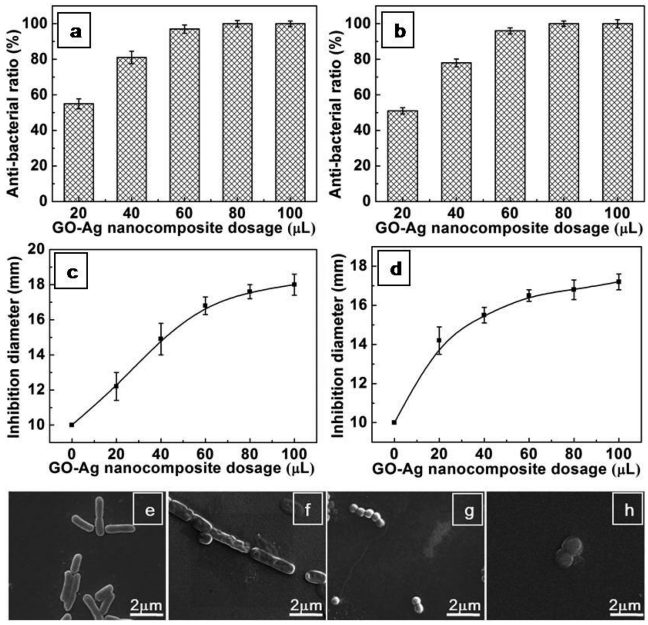

Figure 9. Antibacterial ratios (a and b), comparative inhibition zones (c and d) of GO-Ag nanocomposite with different dosages, morphologies of native bacteria (e and g), and bacteria treated with 100 μL of GO-Ag nanocomposite (f and h): *E. coli* (a, c, e, and f) and *S. aureus* (b, d, g, and h).

Therefore, antibacterial behavior of GO-Ag nanocomposite displayed a dose-dependent manner. These results indicate that GO-Ag nanocomposites have excellent antibacterial activities against Gram negative *E. coli* and Gram positive *S. aureus*.

Antibacterial activity of GO-Ag nanocomposite against *E. coli* and *S. aureus* was further investigated by the disc diffusion method. The prepared GO-Ag nanocomposites were dropped on a sterile filter paper and placed on lawns of tested bacteria in TSA. Antibacterial activity is measured by the clear zone of inhibition around the samples after 24 h incubation and the diameters of zone of inhibition are shown in Figure 9c,d. Between two tested bacteria, *E. coli* has a larger zone of inhibition of 18 mm and *S. aureus* has a smaller zone of inhibition of 17.2 mm for 100 μL dosages of GO-Ag nanocomposite. The differences observed in the diameter of zone of inhibition may be due to the difference in the susceptibility of different bacteria to the prepared GO-Ag nanocomposite. The antibacterial mechanism of AgNPs has not been completely understood yet. The most possible mechanism is due to Ag^+ released from AgNPs, which strongly binds to thiol groups (SH) found in enzymes and proteins on the cellular surface and can interfere with cell division and lead to bacterial cell death.[2] Moreover, AgNPs can cause oxidative damage with producing reactive oxygen species (ROS), leading to attack enzymes and proteins and resulting in irreversible damage to DNA replication.[38] The present study clearly indicates that GO-Ag nanocomposite show excellent antibacterial activity against both Gram negative and positive organisms. Combining all beneficial qualities makes the prepared GO-Ag nanocomposite excellent antibacterial materials that can be applied in biomedical applications.

SEM microscopy was applied to evaluate the surface morphology changes of the native and treated *E. coli* and *S. aureus* (Figure 9e−h) with prepared nanocomposite in TSB. As shown in Figure 9e and g, native *E. coli* and *S. aureus* were

DOI: 10.1021/acsami.5b00937
ACS Appl. Mater. Interfaces 2015, 7, 6966−6973

typically rod-shaped and round-shaped, respectively, both with smooth and intact cell walls.[17] After being treated with GO-Ag nanocomposite, cell walls of *E. coli* (Figure 9f) became wrinkled and damaged with its shape and size of cells changed dramatically, which is similar to previous reports.[39] The similar phenomena also can be seen in *S. aureus* cells (Figure 9h). It is likely that GO-Ag nanocomposite exhibited strong impacts on the cell walls and cell membranes of both Gram positive and Gram negative bacteria, resulting in destroying bacterial cell membrane/wall integrity.[17]

CONCLUSION

In summary, an environmentally friendly, facile, and simple method was developed to synthesize GO-Ag nanocomposite. AgNPs with monodispersed size were well dispersed on the surface of GO nanosheets. Moreover, both GO nanosheets and AgNPs were prevented from the agglomeration with starch as the stabilizer. GO-Ag nanocomposite displayed very low cytotoxicty and showed highly effective antibacterial activities against *E. coli* and *S. aureus*. Nevertheless, the results suggest that GO-Ag nanocomposite could be a promising antibacterial agent with low toxicity to HEK 293 cells. This novel material reported here can be used for different applications in biomaterials.

AUTHOR INFORMATION

Corresponding Authors

*E-mail: w.shao@njfu.edu.cn. Fax: +86-25-85418873. Phone: +86-25-85427024.

*E-mail: zslnl@hotmail.com. Fax: +86-25-85418873. Phone: +86-25-85428840.

Notes

The authors declare no competing financial interest.

ACKNOWLEDGMENTS

The work was financially supported by the National Natural Science Foundation of China (Grant 51401109), the High-Level Talent Project of Nanjing Forestry University (Grant GXL201301), the Major Program of the Natural Science Foundation of Jiangsu Higher Education of China (Grant 14KJB430018), and the Project Funded by the Priority Academic Program Development of Jiangsu Higher Education Institutions (PAPD). The authors would like to acknowledge the Advanced Analysis & Testing Center of Nanjing Forestry University.

REFERENCES

(1) Shao, W.; Zhao, Q. Effect of Corrosion Rate and Surface Energy of Silver Coatings on Bacterial Adhesion. *Colloids Surf., B* **2010**, *76*, 98−103.

(2) de Faria, A. F.; Martinez, D. S. T.; Meira, S. M. M.; de Moraes, A. C. M.; Brandelli, A.; Filho, A. G. S.; Alves, O. L. Anti-Adhesion and Antibacterial Activity of Silver Nanoparticles Supported on Graphene Oxide Sheets. *Colloids Surf., B* **2014**, *113*, 115−124.

(3) Madhavan, P.; Hong, P. Y.; Sougrat, R.; Nunes, S. P. Silver-Enhanced Block Copolymer Membranes with Biocidal Activity. *ACS Appl. Mater. Interfaces* **2014**, *6*, 18497−18501.

(4) Wu, M. C.; Deokar, A. R.; Liao, J. H.; Shih, P. Y.; Ling, Y. C. Graphene-Based Photothermal Agent for Rapid and Effective Killing of Bacteria. *ACS Nano* **2013**, *7*, 1281−1290.

(5) Bao, Q.; Zhang, D.; Qi, P. Synthesis and Characterization of Silver Nanoparticle and Graphene Oxide Nanosheet Composites as a Bactericidal Agent for Water Disinfection. *J. Colloid Interface Sci.* **2011**, *360*, 463−470.

(6) Sahni, G.; Gopinath, P.; Jeevanandam, P. A Novel Thermal Decomposition Approach to Synthesize Hydroxyapatite-Silver Nanocomposites and Their Antibacterial Action against GFP-Expressing Antibiotic Resistant *E. coli*. *Colloids Surf., B* **2013**, *103*, 441−447.

(7) Nguyen, V. H.; Kim, B. K.; Jo, Y. L.; Shim, J. J. Preparation and Antibacterial Activity of Silver Nanoparticles-Decorated Graphene Composites. *J. Supercrit. Fluids* **2012**, *72*, 28−35.

(8) Bindhu, M. R.; Umadevi, M. Antibacterial and Catalytic Activities of Green Synthesized Silver Nanoparticles. *Spectrochim. Acta, Part A* **2015**, *135*, 373−378.

(9) Wei, Y.; Zuo, X.; Li, X.; Song, S.; Chen, L.; Shen, J.; Meng, Y.; Zhao, Y.; Fang, S. Dry Plasma Synthesis of Graphene Oxide-Ag Nanocomposites: A Simple and Green Approach. *Mater. Res. Bull.* **2014**, *53*, 145−150.

(10) Li, Y.; Cao, Y.; Xie, J.; Jia, D.; Qin, H.; Liang, Z. Facile Solid-State Synthesis of Ag/Graphene Oxide Nanocomposites as Highly Active and Stable Catalyst for the Reduction of 4-Nitrophenol. *Catal. Commun.* **2015**, *58*, 21−25.

(11) Wang, X.; Huang, P.; Feng, L.; He, M.; Guo, S.; Shen, G.; Cui, D. Green Controllable Synthesis of Silver Nanomaterials on Graphene Oxide Sheets via Spontaneous Reduction. *RSC Adv.* **2012**, *2*, 3816−3822.

(12) Han, Y.; Luo, Z.; Yuwen, L.; Tian, J.; Zhu, X.; Wang, L. Synthesis of Silver Nanoparticles on Reduced Graphene Oxide under Microwave Irradiation with Starch as an Ideal Reductant and Stabilizer. *Appl. Surf. Sci.* **2013**, *266*, 188−193.

(13) Liao, K. H.; Lin, Y. S.; Macosko, C. W.; Haynes, C. L. Cytotoxicity of Graphene Oxide and Graphene in Human Erythrocytes and Skin Fibroblasts. *ACS Appl. Mater. Interfaces* **2011**, *3*, 2607−2615.

(14) Ruiz, O. N.; Fernando, K. A. S.; Wang, B.; Brown, N. A.; Luo, P. G.; McNamara, N. D.; Vangsness, M.; Sun, Y. P.; Bunker, C. E. Graphene Oxide: A Nonspecific Enhancer of Cellular Growth. *ACS Nano* **2011**, *5*, 8100−8107.

(15) Kavitha, T.; Gopalan, A. I.; Lee, K. P.; Park, S. Y. Glucose Sensing, Photocatalytic and Antibacterial Properties of Graphene-ZnO Nanoparticle Hybrids. *Carbon* **2012**, *50*, 2994−3000.

(16) Dinh, D. A.; Hui, K. S.; Hui, K. N.; Cho, Y. R.; Zhou, W.; Hong, X.; Chun, H. H. Green Synthesis of High Conductivity Silver Nanoparticle-Reduced Graphene Oxide Composite Films. *Appl. Surf. Sci.* **2014**, *298*, 62−67.

(17) Tang, J.; Chen, Q.; Xu, L.; Zhang, S.; Feng, L.; Cheng, L.; Xu, H.; Liu, Z.; Peng, R. Graphene Oxide-Silver Nanocomposite as a Highly Effective Antibacterial Agent with Species-Specific Mechanisms. *ACS Appl. Mater. Interfaces* **2013**, *5*, 3867−3874.

(18) Li, C.; Wang, X.; Chen, F.; Zhang, C.; Zhi, X.; Wang, K.; Cui, D. The Antifungal Activity of Graphene Oxide-Silver Nanocomposites. *Biomaterials* **2013**, *34*, 3882−3890.

(19) Hui, K. S.; Hui, K. N.; Dinh, D. A.; Tsang, C. H.; Cho, Y. R.; Zhou, W.; Hong, X.; Chun, H. H. Green Synthesis of Dimension-Controlled Silver Nanoparticle-Graphene Oxide with in Situ Ultrasonication. *Acta Mater.* **2014**, *64*, 326−332.

(20) Chevirona, P.; Gouanvéa, F.; Espuche, E. Green Synthesis of Colloid Silver Nanoparticles and Resulting Biodegradable Starch/Silver Nanocomposites. *Carbohydr. Polym.* **2014**, *108*, 291−298.

(21) Cai, X.; Tan, S.; Lin, M.; Xie, A.; Mai, W.; Zhang, X.; Lin, Z.; Wu, T.; Liu, Y. Synergistic Antibacterial Brilliant Blue/Reduced Graphene Oxide/Quaternary Phosphonium Salt Composite with Excellent Water Solubility and Specific Targeting Capability. *Langmuir* **2011**, *27*, 7828−7835.

(22) Deetuam, C.; Samthong, C.; Thongyai, S.; Praserthdam, P.; Somwangthanaroj, A. Synthesis of Well Dispersed Graphene in Conjugated Poly(3,4-ethylenedioxythiophene): Polystyrene Sulfonate via Click Chemistry. *Compos. Sci. Technol.* **2014**, *93*, 1−8.

(23) Das, M. R.; Sarma, R. K.; Borah, S. C.; Kumari, R.; Saikia, R.; Deshmukh, A. B.; Shelke, M. V.; Sengupta, P.; Szunerits, S.; Boukherroub, R. The Synthesis of Citrate-Modified Silver Nanoparticles in an Aqueous Suspension of Graphene Oxide Nanosheets and Their Antibacterial Activity. *Colloids Surf., B* **2013**, *105*, 128−136.

DOI: 10.1021/acsami.5b00937
ACS Appl. Mater. Interfaces 2015, 7, 6966−6973

(24) Shao, W.; Liu, H.; Liu, X.; Wang, S.; Zhang, R. Anti-Bacterial Performances and Biocompatibility of Bacterial Cellulose/Graphene Oxide Composites. *RSC Adv.* **2015**, *5*, 4795−4803.
(25) Valentini, L.; Cardinali, M.; Fortunati, E.; Torre, L.; Kenny, J. M. A Novel Method to Prepare Conductive Nanocrystalline Cellulose/Graphene Oxide Composite Films. *Mater. Lett.* **2013**, *105*, 4−7.
(26) Satheesh, K.; Jayavel, R. Synthesis and Electrochemical Properties of Reduced Graphene Oxide via Chemical Reduction Using Thiourea as a Reducing Agent. *Mater. Lett.* **2013**, *113*, 5−8.
(27) Chen, J.; Zheng, X.; Wang, H.; Zheng, W. Graphene Oxide-Ag Nanocomposite: In Situ Photochemical Synthesis and Application as a Surface-Enhanced Raman Scattering Substrate. *Thin Solid Films* **2011**, *520*, 179−185.
(28) Shen, J. F.; Li, T.; Shi, M.; Li, N.; Ye, M. X. Polyelectrolyte-Assisted One-Step Hydrothermal Synthesis of Ag-Reduced Graphene Oxide Composite and Its Antibacterial Properties. *Mater. Sci. Eng., C* **2012**, *32*, 2042−2047.
(29) Tang, X. Z.; Li, X.; Cao, Z.; Yang, J.; Wang, H.; Pu, X.; Yu, Z. Z. Synthesis of Graphene Decorated with Silver Nanoparticles by Simultaneous Reduction of Graphene Oxide and Silver Ions with Glucose. *Carbon* **2013**, *59*, 93−99.
(30) Ma, J.; Zhang, J.; Xiong, Z.; Yong, Y.; Zhao, X. S. Preparation, Characterization and Antibacterial Properties of Silver-Modified Graphene Oxide. *J. Mater. Chem.* **2011**, *21*, 3350−3352.
(31) Martínez-Abad, A.; Lagarón, J. M.; Ocio, M. J. Antimicrobial Beeswax Coated Polylactide Films with Silver Control Release Capacity. *Int. J. Food Microbiol.* **2014**, *174*, 39−46.
(32) Honda, M.; Kawanobe, Y.; Ishii, K.; Konishi, T.; Mizumoto, M.; Kanzawa, N.; Matsumoto, M.; Aizawa, M. In vitro and in vivo Antimicrobial Properties of Silver-Containing Hydroxyapatite Prepared via Ultrasonic Spray Pyrolysis Route. *Mater. Sci. Eng., C* **2013**, *33*, 5008−5018.
(33) Cienchanska, D. Multifunctional Bacterial Cellulose/Chitosan Composite Materials for Medical Applications. *Fibres Text. East. Eur.* **2004**, *12*, 69−72.
(34) Ul-Islam, M.; Khan, T.; Park, J. K. Water Holding and Release Properties of Bacterial Cellulose Obtained by in situ and ex situ Modification. *Carbohydr. Polym.* **2012**, *88*, 596−603.
(35) Peretyazhko, T. S.; Zhang, Q.; Colvin, V. L. Size-Controlled Dissolution of Silver Nanoparticles at Neutral and Acidic pH Conditions: Kinetics and Size Changes. *Environ. Sci. Technol.* **2014**, *48*, 11954−11961.
(36) Purwar, R.; Rajput, P.; Srivastava, C. M. Composite Wound Dressing for Drug Release. *Fibers Polym.* **2014**, *15*, 1422−1428.
(37) Cheng, Y.; Lu, J.; Liu, S.; Zhao, P.; Lu, G.; Chen, J. The Preparation, Characterization and Evaluation of Regenerated Cellulose/Collagen Composite Hydrogel Films. *Carbohydr. Polym.* **2014**, *107*, 57−64.
(38) Markowska, K.; Grudniak, A. M.; Wolska, K. I. Silver Nanoparticles as an Alternative Strategy against Bacterial Biofilms. *Acta Biochim. Polym.* **2013**, *60*, 523−530.
(39) Hu, W.; Peng, C.; Luo, W.; Lv, M.; Li, X.; Li, D.; Huang, Q.; Fan, C. Graphene-Based Antibacterial Paper. *ACS Nano* **2010**, *4*, 4317−4323.

DOI: 10.1021/acsami.5b00937
ACS Appl. Mater. Interfaces 2015, 7, 6966−6973